

Major Groove Orientation of the (2*S*)-*N*⁶-(2-Hydroxy-3-buten-1-yl)-2'-deoxyadenosine DNA Adduct Induced by 1,2-Epoxy-3-butene

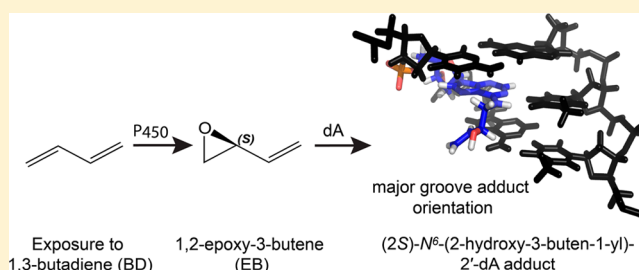
Ewa A. Kowal,[†] Susith Wickramaratne,[‡] Srikanth Kotapati,[‡] Michael Turo,[†] Natalia Tretyakova,[‡] and Michael P. Stone^{*,†}

[†]Department of Chemistry, Center in Molecular Toxicology, Vanderbilt Ingram Cancer Center, and Center for Structural Biology, Vanderbilt University, 2201 West End Avenue, Nashville, Tennessee 37235, United States

[‡]Department of Medicinal Chemistry, Masonic Cancer Center, and Department of Chemistry, University of Minnesota, Minneapolis Minnesota 55455, United States

S Supporting Information

ABSTRACT: 1,3-Butadiene (BD) is an environmental and occupational toxicant classified as a human carcinogen. It is oxidized by cytochrome P450 monooxygenases to 1,2-epoxy-3-butene (EB), which alkylates DNA. BD exposures lead to large numbers of mutations at A:T base pairs even though alkylation of guanines is more prevalent, suggesting that one or more adenine adducts of BD play a role in BD-mediated genotoxicity. However, the etiology of BD-mediated genotoxicity at adenine remains poorly understood. EB alkylates the *N*⁶ exocyclic nitrogen of adenine to form *N*⁶-(hydroxy-3-buten-1-yl)-2'-dA ((2*S*)-*N*⁶-HB-dA) adducts (Tretyakova, N., Lin, Y., Sangaiah, R., Upton, P. B., and Swenberg, J. A. (1997) *Carcinogenesis* 18, 137–147). The structure of the (2*S*)-*N*⁶-HB-dA adduct has been determined in the 5'-d(C¹G²G³A⁴C⁵Y⁶A⁷G⁸A⁹A¹⁰G¹¹)-3':5'-d(C¹²T¹³T¹⁴C¹⁵T¹⁶T¹⁷G¹⁸T¹⁹C²⁰C²¹G²²)-3' duplex [Y = (2*S*)-*N*⁶-HB-dA] containing codon 61 (underlined) of the human *N-ras* protooncogene, from NMR spectroscopy. The (2*S*)-*N*⁶-HB-dA adduct was positioned in the major groove, such that the butadiene moiety was oriented in the 3' direction. At the C_α carbon, the methylene protons of the modified nucleobase Y⁶ faced the 5' direction, which placed the C_β carbon in the 3' direction. The C_β hydroxyl group faced toward the solvent, as did carbons C_γ and C_δ. The C_β hydroxyl group did not form hydrogen bonds with either T¹⁶ O⁴ or T¹⁷ O⁴. The (2*S*)-*N*⁶-HB-dA nucleoside maintained the *anti* conformation about the glycosyl bond, and the modified base retained Watson–Crick base pairing with the complementary base (T¹⁷). The adduct perturbed stacking interactions at base pairs C⁵:G¹⁸, Y⁶:T¹⁷, and A⁷:T¹⁶ such that the Y⁶ base did not stack with its 5' neighbor C⁵, but it did with its 3' neighbor A⁷. The complementary thymine T¹⁷ stacked well with both 5' and 3' neighbors T¹⁶ and G¹⁸. The presence of the (2*S*)-*N*⁶-HB-dA resulted in a 5 °C reduction in the *T*_m of the duplex, which is attributed to less favorable stacking interactions and adduct accommodation in the major groove.



INTRODUCTION

1,3-Butadiene (BD) is a genotoxic chemical strongly carcinogenic in laboratory mice^{1–3} and to a lesser extent in rats.⁴ BD has been classified by the United States Environmental Protection Agency as “carcinogenic to humans by inhalation,”⁵ and it has been also characterized as a known human carcinogen by the National Toxicology Program.⁶ The International Agency for Cancer Research (IARC) lists BD as “carcinogenic to humans (Group 1).”^{7,8} Accordingly, there has been interest in identifying human biomarkers of exposure to BD.^{9,10} These exposures arise occupationally during the manufacture of styrene–butadiene rubber^{11,12} and also environmentally since BD is found in automobile emissions¹³ and in cigarette smoke.¹⁴ Chronic exposures to BD may induce genotoxic effects^{15–17} and have been associated with increased cancer risk.^{11,18–26}

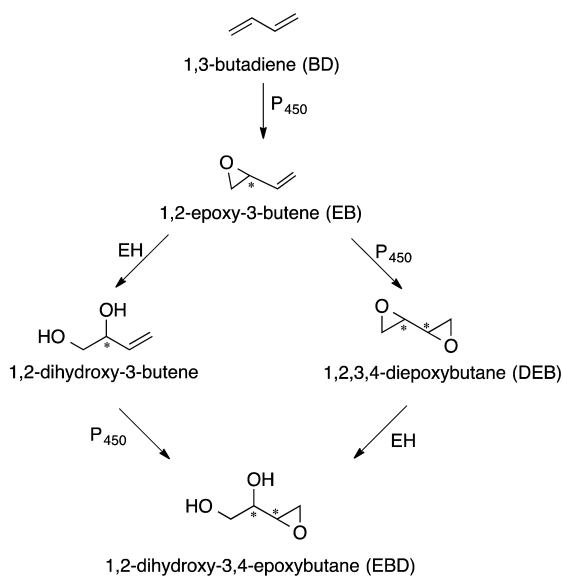
Albertini, Kirman, and co-workers have reviewed BD metabolism and genotoxicity.^{27–29} It is of interest that BD

exposures lead to large numbers of mutations at A:T base pairs,^{30–34} even though alkylation of guanines by EB is more prevalent.³⁵ The number of A:T base pair substitutions has been reported to equal or exceed the number of mutations at G:C base pairs,³⁴ which implies that one or more adenine-specific lesions contribute significantly to butadiene-induced genotoxicity.^{32,34,36} However, the etiology of adenine-specific mutations remains incompletely understood.^{32,37,38} Electrophilic 1,2-epoxy-3-butenes (EB) are formed prevalently when BD is oxidized by cytochrome P450 enzymes (Scheme 1),^{39–41} and alkylation products formed from the reactions of EB with adenine have been characterized. In each instance, a pair of regioisomeric 1-hydroxy-3-buten-2-yl and 2-hydroxy-3-buten-1-yl and alkylation products is produced as a result of epoxide ring opening at either the internal or the terminal carbon atoms

Received: April 30, 2014

Published: September 19, 2014

Scheme 1. Cytochrome P₄₅₀-Mediated Oxidation of BD to EB, DEB, and EBD, Where EH Is Epoxide Hydrolase

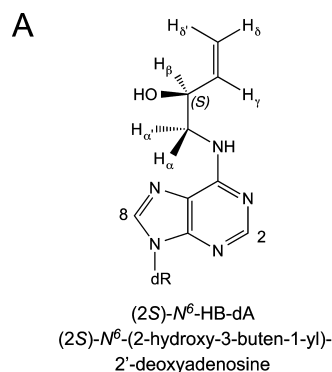


of EB, respectively. Among the EB-dA products that have been identified in calf thymus DNA are *N*-1-(1-hydroxy-3-buten-2-yl)-adenine, *N*-1-(2-hydroxy-3-buten-1-yl)-adenine, *N*-3-(1-hydroxy-3-buten-2-yl)-adenine, and *N*-3-(2-hydroxy-3-buten-1-yl)-adenine. The N1-dA and N3-dA adducts occur at lower levels than do N7-dG adducts,³⁹ but they may be important for the ability of EB to induce mutations at A:T base pairs.^{30–34}

The N1-dA adducts are likely to be precursors of the regioisomeric *N*⁶-(1-hydroxy-3-buten-2-yl)-2'-dA adducts⁴² and *N*⁶-(2-hydroxy-3-buten-1-yl)-dA (*N*⁶-HB-dA) adducts (Chart 1) through Dimroth rearrangement.^{39,43–45} *N*⁶-HB-dA adducts have been detected in calf thymus DNA treated with EB *in vitro*.^{42,46,47} *N*⁶-HB-dA adducts have also been detected in tissues of rodents exposed to BD by inhalation.^{46,48} A second P450-catalyzed oxidation of EB leads to the more genotoxic diepoxybutane (DEB),^{7,12,30–32} a bis-electrophile that forms DNA–DNA cross-links^{49–54} and DNA–protein conjugates.⁵⁰ Thus, proximate electrophiles arising from BD metabolism include not only EB, and also DEB, and 1,2-dihydroxy-3,4-epoxybutane (EBD).^{55–57} Additionally, EBD is metabolized by cytochrome P450 to hydroxymethylvinylketones (HMVK).^{58,59}

The preparation of site-specific BD alkylation products in synthetic oligodeoxynucleotides provides a basis by which to probe the chemistry and biology of BD-derived electrophiles in DNA. The potential roles of both regio- and stereochemistry in modulating processing of these adducts are of interest, e.g., in light of the regio- and stereospecific processing of adducts arising from diol epoxides of various polycyclic aromatic hydrocarbons.⁶⁰ Harris and co-workers developed a post-oligomerization synthetic approach^{61,62} in which oligodeoxynucleotides modified site-specifically with 6-chloropurine were reacted with regio- and stereospecific amino alcohol surrogates of specific BD-derived adducts.⁶³ Following this approach, oligodeoxynucleotides containing site-specific *N*⁶-(2-hydroxy-3-buten-1-yl)-dA (*N*⁶-HB-dA) adducts have been prepared by Quirk-Dorr et al.⁶⁴ The ras61 duplex 5'-d(CGGACAAGAAG)-3':5'-d(CTTCTTGTCCG)-3' contains codons 60, 61 (underlined), and 62 of the human N-ras protooncogene. Feng and Stone⁶⁵ employed a restrained molecular dynamics and

Chart 1. (A) Structure of the (2*S*)-*N*⁶-HB-dA Adduct and (B) Sequences and Numbering of the Unmodified and Modified Duplexes^a



B Unmodified duplex

5' -d(C¹ G² G³ A⁴ C⁵ A⁶ A⁷ G⁸ A⁹ A¹⁰ G¹¹) -3'
3' -d(G²² C²¹ C²⁰ T¹⁹ G¹⁸ T¹⁷ T¹⁶ C¹⁵ T¹⁴ T¹³ C¹²) -5'

Modified duplex

5' -d(C¹ G² G³ A⁴ C⁵ Y⁶ A⁷ G⁸ A⁹ A¹⁰ G¹¹) -3'
3' -d(G²² C²¹ C²⁰ T¹⁹ G¹⁸ T¹⁷ T¹⁶ C¹⁵ T¹⁴ T¹³ C¹²) -5'

Y = (2*S*)-*N*⁶-HB-dA

^aIn A, H_α is the pro-R, and H_{α'} is the pro-S proton. In B, at the Y⁶ position adenine has been replaced with the (2*S*)-*N*⁶-HB-dA adduct to form the modified duplex.

simulated annealing approach to refine the structure of this duplex and concluded that it maintained a B-like DNA helix.

In the present work, we have generated DNA strands containing site- and stereospecific *N*⁶-HB-dA adducts of BD. The structure of the (2*S*)-*N*⁶-HB-dA adduct⁶⁴ has been determined in the ras61 5'-d(C¹G²G³A⁴C⁵Y⁶A⁷G⁸A⁹A¹⁰G¹¹)-3':5'-d(C¹²T¹³T¹⁴C¹⁵T¹⁶T¹⁷G¹⁸T¹⁹C²⁰C²¹G²²)-3' duplex [Y = (2*S*)-*N*⁶-HB-dA] (Chart 1). The structure reveals that the (2*S*)-*N*⁶-HB-dA adduct is positioned in the major groove such that the butadiene moiety is oriented in the 3' direction. The modified base Y⁶ maintains Watson–Crick base pairing with the complementary base T¹⁷. The (2*S*)-*N*⁶-HB-dA adduct perturbs stacking interactions at base pairs C⁵:G¹⁸, Y⁶:T¹⁷, and A⁷:T¹⁶ resulting in a 5 °C reduction in the *T*_m of the duplex.

■ MATERIALS AND METHODS

Syntheses and Characterization of Oligodeoxynucleotides.

Unmodified oligodeoxynucleotides 5'-d(CGGACAAGAAG)-3' and 5'-d(CTTCTTGTCCG)-3' were synthesized by the Midland Reagent Company (Midland, TX) and purified by anion-exchange HPLC. The 5'-O-(4,4'-dimethoxytrityl)-3'-O-(2-cyanoethyl)-*N,N*-diisopropyl phosphoramidite of 6-chloropurine-2'-deoxyribonucleoside was purchased from ChemGenes Co. (Wilmington, MA). The 2'-deoxyribonucleoside-3'-phosphoramidites and all other reagents necessary for automated DNA synthesis were purchased from Glen Research (Sterling, VA). Oligodeoxynucleotides were synthesized by solid phase methods using an ABI 394 DNA synthesizer (Life Technologies, Carlsbad, CA). All solvents and chemical reagents were obtained from commercial sources and used without further purification. The oligodeoxynucleotide 5'-d(CGGAC^YAGAAG)-3' containing the (2*S*)-*N*⁶-HB-dA adduct was synthesized by coupling 6-chloropurine containing DNA with 1-aminobut-3-en-2-ol.⁶⁴ Briefly, an 11-mer oligodeoxynucleotide containing a 6-chloropurine at position Y⁶ (210 nmol) was coupled with 1-aminobut-3-en-2-ol

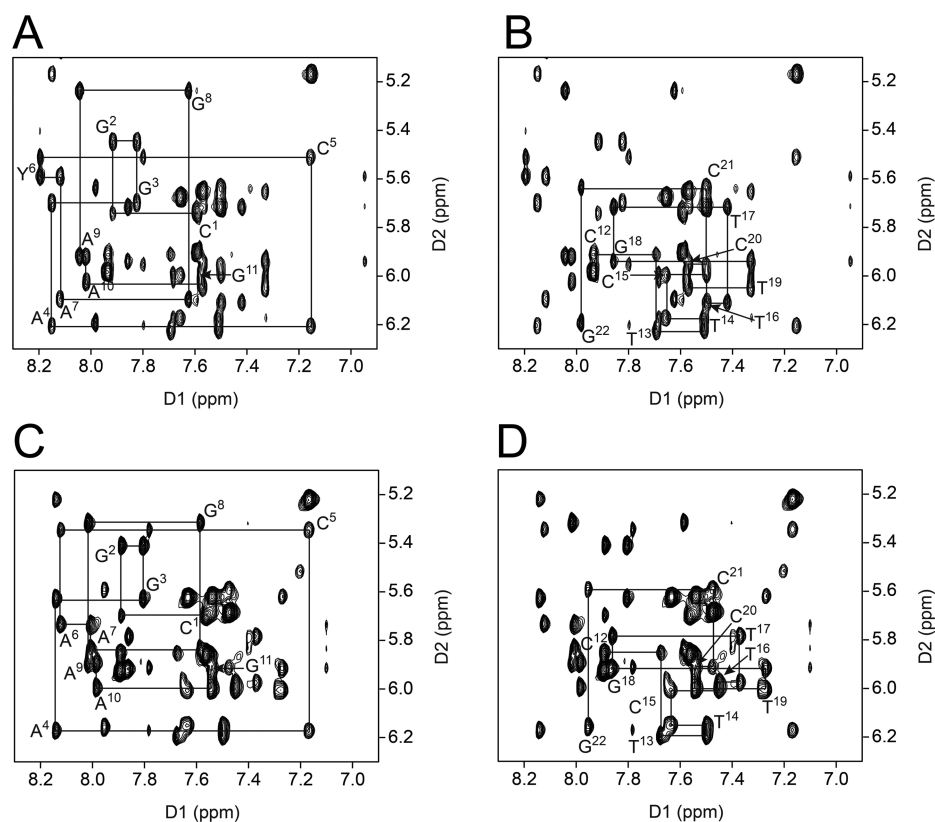


Figure 1. NOESY spectra for the modified and unmodified duplexes, showing sequential NOEs between the base aromatic and anomeric protons. (A) The (2*S*)-*N*⁶-HB-dA modified duplex, showing nucleotides C¹ to G¹¹. The resonance at 6.95 ppm (D1) belongs to the Y⁶ H2 proton. (B) The (2*S*)-*N*⁶-HB-dA modified duplex, showing nucleotides C¹² to G²². (C) The unmodified duplex, showing nucleotides C¹ to G¹¹. The resonance at 7.10 ppm (D1) belongs to the A⁶ H2 proton. (D) The unmodified duplex, showing nucleotides C¹² to G²². Spectra were obtained at 800 and 600 MHz for modified and unmodified duplexes, respectively, both with a mixing time of 250 ms at 15 °C.

(7.44 mg), in the presence of DIPEA (210 μ L) in DMSO (700 μ L) for 16 h at 60 °C. The oligodeoxynucleotides were purified using semipreparative reverse-phase HPLC (YMC, Kyoto, Japan, Phenyl-Hexyl, 5 μ m, 250 mm \times 10.0 mm) equilibrated with 0.1 M ammonium formate (pH 7.0) using an acetonitrile gradient. The oligodeoxynucleotides were desalted using Sephadex G-25 and lyophilized. The adducted oligodeoxynucleotides were characterized by capillary HPLC–ESI–MS. Sequence and site-specificity were confirmed by MALDI-TOF-MS of partial exonuclease digests. The unmodified oligodeoxynucleotides were characterized by capillary HPLC–ESI–MS. The concentrations of single-stranded oligodeoxynucleotides were determined by UV absorbance at 260 nm using extinction coefficients of 118,300 L M⁻¹cm⁻¹ for 5'-d(CGGACYAGAAG)-3' and 5'-d(CGGACAAGAAG)-3' and 90,800 L M⁻¹cm⁻¹ for the complementary strand 5'-d(CTTCTTGTCGG)-3'.⁶⁶ Equimolar quantities of the complementary strands were combined and annealed by heating to 80 °C for 15 min and then slowly cooled to room temperature to form a duplex.

DNA Melting Studies. Absorption vs temperature profiles for each duplex were measured using a Varian Cary 100 Bio spectrophotometer (Varian Associates, Palo Alto, CA). The concentrations of the duplexes were 1.24 μ M. Samples were prepared in a solution of 10 mM NaH₂PO₄ and 50 μ M Na₂EDTA containing 0.1 M NaCl (pH 7.0). The temperature was increased from 5 to 90 °C for each duplex at a rate of 1.0 °C/min. The UV absorbance was monitored at 260 nm. The *T*_m values were determined by taking the first derivatives of the melting curves and shape analyses.

NMR Spectroscopy. The DNA duplex containing the Y⁶ adduct was prepared at 0.51 mM concentration in 0.1 M NaCl and 50 μ M Na₂EDTA in the presence of 10 mM NaH₂PO₄ (pH 7.0). To observe nonexchangeable protons, the duplex was exchanged with D₂O and dissolved in 99.96% D₂O. To observe exchangeable protons, the

duplex was dissolved in 9:1 H₂O/D₂O. ¹H NMR spectra were recorded using 800 and 600 MHz spectrometers equipped with cryogenic probes (Bruker Biospin, Billerica, MA). Chemical shifts were referenced to the chemical shift of water at the corresponding temperature, with respect to 4,4-dimethyl-4-silapentane-1-sulfonic acid (DSS). Data were processed using TOPSPIN (Bruker Biospin Inc., Billerica, MA). NOESY^{67,68} and DQF-COSY⁶⁹ spectra in D₂O were collected at 15 °C at 800 MHz; NOESY experiments were conducted at a mixing time of 60 and 250 ms. These experiments were performed with a relaxation delay of 2.0 s. The NOESY spectrum in 9:1 H₂O/D₂O was collected at 10 °C at 600 MHz for the modified and unmodified duplexes with a 250 ms mixing time. NMR experiments as a function of temperature in 9:1 H₂O/D₂O solution were collected at 5, 10, 15, 20, 25, and 30 °C at 600 MHz. These experiments were performed with a relaxation delay of 1.5 s. Water suppression was performed using the WATERGATE pulse sequence.⁷⁰ The cross-peaks were assigned using the program SPARKY.⁷¹

NMR Distance Restraints. NOESY spectra cross-peak volumes were measured by volume integrations of the NOESY spectra using SPARKY. They were divided into five classes based on confidence in the integrations. The intrinsic integration error was assigned to be one-half the volume of the cross-peak of lowest intensity. The overlapping of cross-peaks, spectroscopic line broadening of cross-peaks, which was particularly an issue for integrations of cross-peaks involving exchangeable protons, and the potential for spin diffusion provided additional sources of integration errors. The class 1 cross-peak volumes were derived from well-resolved strong nonoverlapping cross-peaks and were assigned 10% error. The class 2 cross-peak volumes were derived from strong but slightly overlapped cross-peaks and were assigned 20% error. The class 3 cross-peak volumes were derived from strong but medially overlapped cross-peaks and were assigned 30% error. Classes 4 and 5 of the cross-peak volumes were derived from

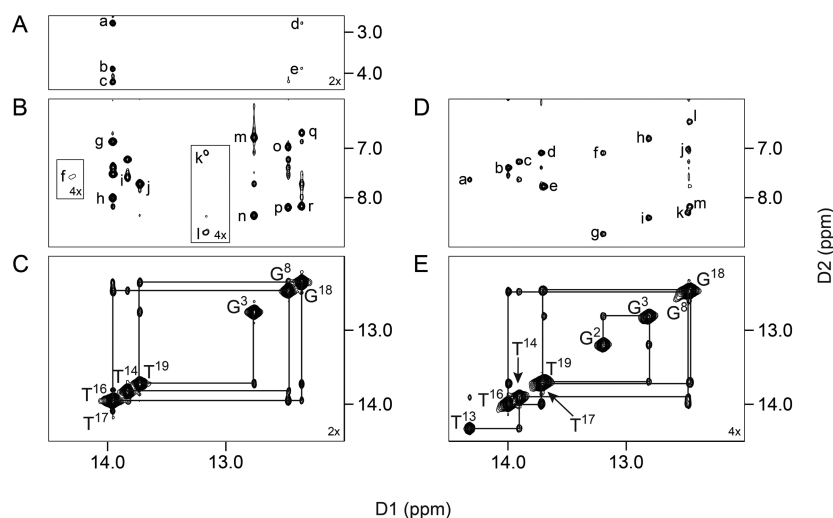


Figure 2. NOESY spectra for the (2S)- N^6 -HB-dA modified (A–C) and unmodified (D–E) duplexes, showing NOEs between the base imino protons and the amino protons. (A) Interstrand NOEs between the Y^6 adduct and the T^{17} base. The cross-peaks are assigned as a, $Y^6 H_{\alpha'} \rightarrow T^{17} N3H$; b, $Y^6 H_{\beta} \rightarrow T^{17} N3H$; c, $Y^6 H_{\beta} \rightarrow T^{17} N3H$; d, $Y^6 H_{\alpha'} \rightarrow G^{18} N1H$; and e, $Y^6 H_{\alpha'} \rightarrow G^{18} N1H$. (B) Interstrand NOEs between complementary bases. The cross-peaks are assigned as f, $A^{10} H2 \rightarrow T^{13} N3H$; g, $Y^6 H2 \rightarrow T^{17} N3H$; h, $A^7 H2 \rightarrow T^{16} N3H$; i, $A^9 H2 \rightarrow T^{14} N3H$; j, $A^4 H2 \rightarrow T^{19} N3H$; k, $C^{21} N^4H1 \rightarrow G^2 N1H$; l, $C^{21} N^4H2 \rightarrow G^2 N1H$; m, $C^{20} N^4H1 \rightarrow G^3 N1H$; n, $C^{20} N^4H2 \rightarrow G^3 N1H$; o, $C^{15} N^4H1 \rightarrow G^8 N1H$; p, $C^{15} N^4H2 \rightarrow G^8 N1H$; q, $C^5 N^4H1 \rightarrow G^{18} N1H$; and r, $C^5 N^4H2 \rightarrow G^{18} N1H$. (C) NOE connectivity for the imino protons for the base pairs $G^2:C^{21}$, $G^3:C^{20}$, $A^4:T^{19}$, $C^5:G^{18}$, $Y^6:T^{17}$, $A^7:T^{16}$, $G^8:C^{15}$, and $A^9:T^{14}$. The cross-peaks are $T^{14} N3H \rightarrow G^8 N1H$, $G^8 N1H \rightarrow T^{16} N3H$, $T^{16} N3H \rightarrow T^{17} N3H$, $T^{17} N3H \rightarrow G^{18} N1H$, $G^{18} N1H \rightarrow T^{19} N3H$, and $T^{19} N3H \rightarrow G^3 N1H$. The spectrum was obtained at 600 MHz with a mixing time of 250 ms at 10 °C. (D) Interstrand NOEs between complementary bases. The cross-peaks are assigned as a, $A^{10} H2 \rightarrow T^{13} N3H$; b, $A^7 H2 \rightarrow T^{16} N3H$; c, $A^9 H2 \rightarrow T^{14} N3H$; d, $A^6 H2 \rightarrow T^{17} N3H$; e, $A^4 H2 \rightarrow T^{19} N3H$; f, $C^{21} N^4H1 \rightarrow G^2 N1H$; g, $C^{21} N^4H2 \rightarrow G^2 N1H$; h, $C^{20} N^4H1 \rightarrow G^3 N1H$; i, $C^{20} N^4H2 \rightarrow G^3 N1H$; j, $C^{15} N^4H1 \rightarrow G^8 N1H$; k, $C^{15} N^4H2 \rightarrow G^8 N1H$; l, $C^5 N^4H1 \rightarrow G^{18} N1H$; and m, $C^5 N^4H2 \rightarrow G^{18} N1H$. (E) NOE connectivity for the imino protons for the base pairs $G^2:C^{21}$, $G^3:C^{20}$, $A^4:T^{19}$, $C^5:G^{18}$, $A^6:T^{17}$, $G^8:C^{15}$, $A^9:T^{14}$, and $A^{10}:T^{13}$. The cross-peaks are shown as $T^{13} N3H \rightarrow T^{14} N3H$, $T^{14} N3H \rightarrow G^8 N1H$, $G^8 N1H \rightarrow T^{16} N3H$, $T^{16} N3H \rightarrow T^{17} N3H$, $T^{17} N3H \rightarrow G^{18} N1H$, $G^{18} N1H \rightarrow T^{19} N3H$, $T^{19} N3H \rightarrow G^3 N1H$, and $G^3 N1H \rightarrow G^2 N1H$. The spectrum was obtained at 600 MHz with a mixing time of 250 ms at 10 °C.

low S/N, broadened, and/or highly overlapped cross-peaks, such as those in regions close to the water resonance or to the diagonal line of the spectrum. These were assigned 40% and 50% errors, respectively. An unmodified B-type DNA duplex was constructed using the program INSIGHT II (Accelrys Inc., San Diego, CA). The adenine at position A^6 was replaced by the (2S)- N^6 -HB-dA adduct. Partial charges for the (2S)- N^6 -HB-dA base were calculated with the B3LYP/6-31G* basis set in Gaussian.⁷² These were employed in the parameter files prepared in the program XLEAP.⁷³ Table S1 in the Supporting Information provides the parametrization for the modified (2S)- N^6 -HB-dA nucleotide. The modified duplex was subjected to 1000 cycles of potential energy minimization. The integrated cross-peak intensities, separated into five classes, as described above, were combined by the program MARDIGRAS with volumes calculated from complete relaxation matrix analysis of the starting model to generate a hybrid intensity matrix.^{74,75} The program MARDIGRAS was employed to refine the hybrid intensity matrix⁷⁶ and calculate interproton distance vectors, with upper and lower bounds to each distance vector. For methyl protons, the JUMP 3⁷⁷ model was employed. These calculations were performed at 2, 3, and 4 ns isotropic correlation times.

Restrained Molecular Dynamics Calculations. The interproton distance vectors calculated by MARDIGRAS were used to provide distance restraints used in the restrained molecular dynamics (rMD) calculations. The widths of the distance restraint potential energy wells corresponded to the upper and lower bounds on the inter proton distance vectors as calculated by MARDIGRAS. Additional phosphodiester backbone restraints and deoxyribose pseudorotation restraints were employed, derived from B-DNA.⁷⁸ For the modified nucleotide Y^6 , the square potential energy wells for phosphodiester restraints were assigned as $\pm 120^\circ$. For unmodified nucleotides, the widths of the square potential energy wells for the phosphodiester restraints were assigned as $\pm 60^\circ$. The pseudorotation restraints were not employed for the modified nucleotide Y^6 or for the terminal bases C^1 , G^{11} , C^{12} ,

and G^{22} . Watson–Crick base pair restraints were employed for all base pairs.

The simulated annealing protocol⁷⁹ used for the rMD calculations utilized the program AMBER⁸⁰ and the parm99 force field.⁸¹ Force constants of 32 kcal mol⁻¹ Å⁻² were applied for all restraints. The generalized Born model⁸² was used for solvation. The salt concentration was 0.1 M. The molecule was coupled to the bath temperature to establish the temperature during calculations.⁸³ Initially, calculations were performed for 20 ps (20,000 steps). For the first 1,000 steps, the system was heated from 0 to 600 K with a coupling of 0.5 ps, followed by 1,000 steps at 600 K, followed by 16,000 steps in which the system was cooled to 100 K with a coupling of 4 ps. In the last 2,000 steps, additional cooling was applied from 100 to 0 K with a coupling of 1 ps. Subsequently, a 100,000 step calculation was performed over 100 ps. For the first 5,000 steps, the system was heated from 0 to 600 K with a coupling of 0.5 ps, followed by 5,000 steps at 600 K, followed by 80,000 during which the system was cooled to 100 K with a coupling of 4 ps, followed by additional cooling for the last 10,000 steps with a coupling of 1 ps. Structure coordinates were saved after each cycle. Complete relaxation matrix analysis (CORMA)^{74,75} was used to compare intensities calculated from these emergent structures with the experimentally measured distances. Nine structures were chosen, based on the lowest deviations from the experimental distance and dihedral restraints. These were subjected to potential energy minimization and used to obtain an average refined structure.

Data Deposition. The structure factors and coordinates were deposited in the Protein Data Bank (www.rcsb.org). The PDB ID code for the duplex containing the (2S)- N^6 -HB-dA adduct is 2MNX.

RESULTS

NMR Spectroscopy. Base Proton Assignments. Figure 1 shows the regions of the NOESY spectra including the base aromatic proton resonances and deoxyribose H1' proton

resonances^{84,85} for the modified duplex (panels A and B), in comparison with the corresponding unmodified duplex (panels C and D). The presence of the (2*S*)-*N*⁶-HB-dA adduct induced small changes in the sequential pattern of NOEs between the aromatic base protons and the anomeric protons for either strand of the duplex, as compared to the unmodified duplex. For the modified strand, the C⁵ H6 → C⁵ H1', C⁵ H1' → Y⁶ H8, Y⁶ H8 → Y⁶ H1', and Y⁶ H1' → A⁷ H8 NOEs were of similar intensities as compared to the corresponding NOEs arising from distal nucleotides. The intensity of the Y⁶ H8 → Y⁶ H1' NOE was indicative of minimal change in the conformation of the glycosyl torsion angle at the site of modification. For the complementary strand, the T¹⁶ H6 → T¹⁶ H1', T¹⁶ H1' → T¹⁷ H6, T¹⁷ H6 → T¹⁷ H1', and T¹⁷ H1' → G¹⁸ H8 NOEs were of similar intensities compared to the corresponding NOEs from nucleotides distal to the adduct. With the deoxyribose H1' assignments in hand, the remainder of the deoxyribose protons were assigned from a combination of NOESY and COSY data. The adenine H2 proton resonances were assigned based upon NOEs to the thymine N1H imino proton resonances of the respective A:T base pairs. The assignments of the nonexchangeable DNA protons are summarized in Table S2 of the Supporting Information.

Imino and Amino Proton Assignments. Figure 2 shows the regions of the NOESY spectra yielding the assignments of the Watson–Crick hydrogen bonded guanine and thymine imino resonances, and the adenine *N*⁶ and cytosine *N*⁴ exocyclic amino resonances, for the modified duplex in comparison with the unmodified duplex. In the NOESY spectrum of the modified duplex collected at 10 °C, the T¹⁶ and T¹⁷ N3H imino resonances overlapped. For the modified duplex, the sequential pattern of cross-peaks between imino protons⁸⁶ was observed for base pairs G³:C²⁰ → A⁴:T¹⁹ → C⁵:G¹⁸ → Y⁶:T¹⁷ → A⁷:T¹⁶ → G⁸:C¹⁵ → A⁹:T¹⁴ (Figure 2, panel C). The NOEs between the base imino and amino protons for G:C base pairs showed cross-peaks for all base pairs, with the exceptions of the terminal base pairs C¹:G²² and G¹¹:C¹² (Figure 2, panel B). These cross-peaks for the G²:C²¹ base pair were weak (Figure 2, panel B, cross-peaks k and l, plotted at 4× the contour level). The NOEs between the base imino and adenine H2 protons for T:A base pairs showed cross-peaks for all base pairs. The cross-peak between T¹³ N3H and A¹⁰ H2 was of low intensity (Figure 2, Panel B, cross-peak a, plotted at 4× the contour level). The Y⁶ H2 → T¹⁷ N3H cross-peak was of similar intensity compared to the other cross-peaks (g, Figure 2, panel B). The chemical shifts of the imino and amino protons are provided in Table S3 of the Supporting Information.

(2*S*)-*N*⁶-HB-dA Proton Assignments. Six resonances were observed between 2.8 and 5.9 ppm (Figure 3). The H_γ resonance was identified at 5.89 ppm. The H_δ proton, identified at 5.30 ppm, and the H_{δ'} proton, identified at 5.41 ppm, were assigned from their coupling constants to the H_γ proton. The H_{δ'} proton exhibited the larger coupling constant to the H_γ proton (Figure 3). The diastereotopic H_α and H_{α'} resonances of the methylene group were assigned based on the intensities of NOE cross-peaks to the H_β proton and to the Y⁶ H8 proton. The H_α resonance was located at 3.96 ppm, while the H_{α'} resonance was located at 2.86 ppm. The H_β resonance was located at 4.29 ppm. The H_α proton gave a more intense NOE cross-peak to H_β than did H_{α'}. Likewise, the H_{α'} proton gave a more intense NOE cross-peak to the Y⁶ H8 proton than did H_α. Both the H_α and H_{α'} protons exhibited strong NOEs to the C⁵ H5 and H6 protons. The H_β proton exhibited a strong NOE

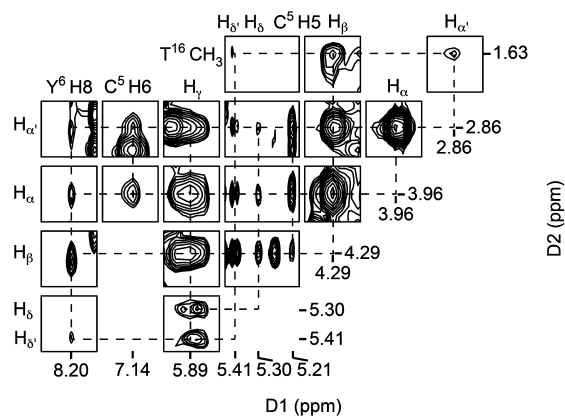


Figure 3. Expanded plot of the NOESY spectrum of the (2*S*)-*N*⁶-HB-dA modified duplex, showing assignments of the adduct protons and cross-peaks from the adduct protons to neighbor base protons. The chemical shifts for each proton are Y⁶ H8, 8.20 ppm; C⁵ H6, 7.14 ppm; Y⁶ H_γ, 5.89 ppm; Y⁶ H_δ, 5.41 ppm; Y⁶ H_δ', 5.30 ppm; C⁵ H5, 5.21 ppm; Y⁶ H_β, 4.29 ppm; Y⁶ H_α, 3.96 ppm; Y⁶ H_α', 2.86 ppm; and T¹⁶ CH₃, 1.63 ppm. The dashed lines show the NOE connectivity for each proton. Cross-peak Y⁶ H8–Y⁶ H_β is overlapped with Y⁶ H8–Y⁶ H_α'. The spectrum was obtained at 800 MHz, with a mixing time of 250 ms and at 15 °C.

to the T¹⁶ CH₃ protons, located in the 3'-neighbor A⁷:T¹⁶ base pair. Weak interstrand NOEs were observed between H_α H_{α'} and H_β and the T¹⁷ N3H imino proton, as well as H_α H_{α'} and the G¹⁸ N1H imino proton (Figure 2, panel A).

Chemical Shift Perturbations. A number of chemical shift perturbations were observed in the modified duplex as compared to the unmodified duplex (Figures 1 and 4). The C⁵ H1' resonance shifted 0.16 ppm downfield, the Y⁶ H8 resonance shifted less than 0.1 ppm downfield, the Y⁶ H2 resonance shifted 0.15 ppm upfield, and the A⁷ H1' and H8 resonances shifted 0.25 and 0.1 ppm downfield. The Y⁶ H1' resonance shifted 0.15 ppm upfield. For the complementary strand of DNA, the largest chemical shift changes were observed for the T¹⁶ H1' resonance, which shifted 0.15 ppm downfield, and for the T¹⁶ H6 resonance, which shifted 0.12 ppm upfield. In the imino proton region of the spectrum, the greatest chemical shift perturbation was observed for the T¹⁷ N3H resonance, which shifted 0.24 ppm downfield as compared to the unmodified duplex (Figure 2).

Thermal Melting Studies. The unfolding of the duplexes was examined by temperature-dependent UV spectroscopy monitored at 260 nm. Incorporation of the (2*S*)-*N*⁶-HB-dA adduct resulted in a 5 °C reduction in the *T*_m value of the duplex. At the concentration of 1.24 μM in 0.1 M NaCl at pH 7, the *T*_m for the unmodified duplex was 44 °C, whereas the *T*_m for the modified duplex was 39 °C. In ¹H NMR experiments collected as a function of temperature from 5 to 30 °C, the T¹⁶ and T¹⁷ N3H and G¹⁸ N1H imino proton resonances remained sharp as compared to the other imino proton resonances as temperature was increased, which suggested that over this range of temperatures, the presence of the modified (2*S*)-*N*⁶-HB-dA base did not increase the rates of exchange with solvent for the C⁵:G¹⁸, Y⁶:T¹⁷, and A⁷:T¹⁶ base pairs (Figure 5).

Structural Refinement. A total of 284 distance restraints obtained from the analyses of the NOESY spectra of nonexchangeable protons were used for restrained molecular dynamics (rMD) calculations.^{74–76} Of these, 126 were internucleotide restraints, and 158 were intranucleotide

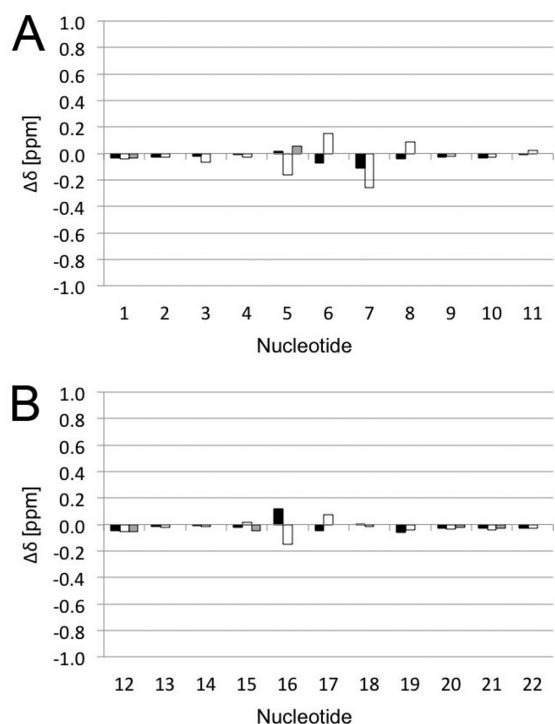


Figure 4. Chemical shift perturbations for the (2S)-N⁶-HB-dA modified duplex compared to those of the unmodified duplex. (A) Strands 1–11, (B) strands 12–22 for aromatic H6/H8 (shown in black), cytosine H5 (gray), and H1' (white) protons, where $\Delta\delta$ [ppm] = $\delta_{\text{Unmodified}}$ [ppm] - δ_{Modified} [ppm].

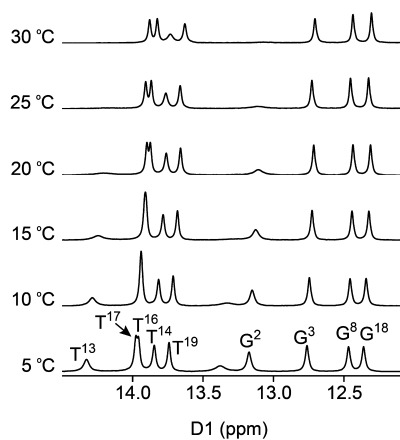


Figure 5. NMR spectra showing the imino proton resonances for the (2S)-N⁶-HB-dA duplex, as a function of temperature. The individual nucleotides are identified by superscripts. The spectra were obtained at 600 MHz, at temperatures 5, 10, 15, 20, 25, and 30 °C.

restraints. As the NMR data were consistent with a right-handed helical DNA duplex similar to that of the canonical B-form DNA,⁷⁸ a total of 90 backbone torsion angles, 45 hydrogen bondings, and 17 deoxyribose pseudorotations were included as empirical restraints in the rMD calculations. Table 1 summarizes the restraints that were used and the refinement statistics.

The rMD calculations employed a simulated annealing protocol.^{79,87} Nine structures emergent from the calculations were subjected to potential energy minimization. Figure 6 shows these nine superimposed structures. Table 2 summarizes the structural statistics. A satisfactory convergence was

Table 1. NMR Restraints Used for the rMD Structural Refinement of the (2S)-N⁶-HB-dA Modified Duplex and the Refinement Statistics

NMR restraints	
NOE restraints	
internucleotide	126
intranucleotide	158
total	284
backbone torsion angle restraints	90
hydrogen bonding distance restraints	45
deoxyribose pseudorotation restraints	17
total number of restraints	436
refinement statistics	
number of distance restraint violations > 0.025 Å	7
number of torsion restraint violations	10
total distance penalty/maximum penalty [kcal mol ⁻¹]	0.776/0.289
total torsion penalty/maximum penalty [kcal mol ⁻¹]	0.490/0.159
r.m.s. distances (Å)	0.012
r.m.s. angles (deg)	2.355
distance restraint force constant [kcal mol ⁻¹ Å ⁻²]	32
torsion restraint force constant [kcal mol ⁻¹ deg ⁻²]	32

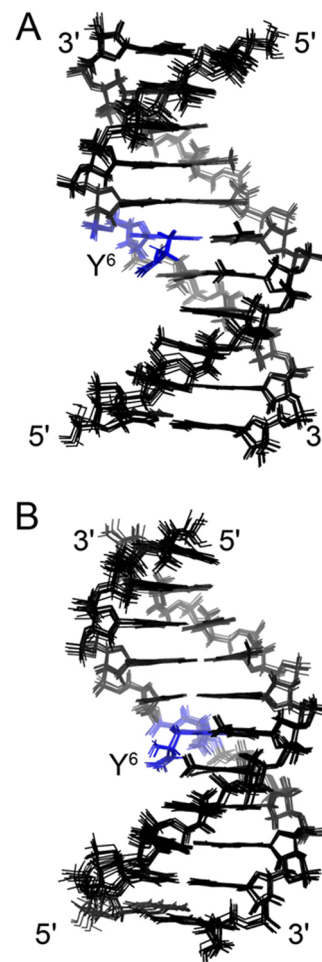


Figure 6. Superpositions of nine structures obtained from a series of rMD calculations for the (2S)-N⁶-HB-dA modified duplex. The modified base Y⁶ is shown in blue. (A) View from the major groove. (B) Side view.

observed, with a maximum pairwise rmsd between the nine structures of 0.53 Å. These nine structures were averaged, and

Table 2. Structural Statistics for the (2*S*)-*N*⁶-HB-dA Modified Duplex

average structure (obtained from 9 structures)	
RMS pairwise difference between structures [Å]	0.53
RMS difference from average structure [Å]	0.35
CORMA analysis for average structure ^a	
$R_1^{x^b}$	
intranucleotide	0.074
internucleotide	0.095
total	0.082
average error ^c	0.018

^aThe mixing time was 250 ms. ^b R_1^x is the sixth root R factor: $\Sigma[(I_o)_i^{1/6} - ((I_c)_i^{1/6})/\Sigma((I_o)_i^{1/6})]$. ^cAverage error: $\Sigma(I_c - I_o)/n$, where I_c are NOE intensities calculated from refined structure, I_o are experimental NOE intensities.

the resulting average structure was subjected to complete relaxation matrix analysis.⁷⁴ The results are shown in Figure 7. The sixth root residuals (R_1^x values) remained consistently below 15%, for both intranucleotide NOEs and internucleotide NOEs.

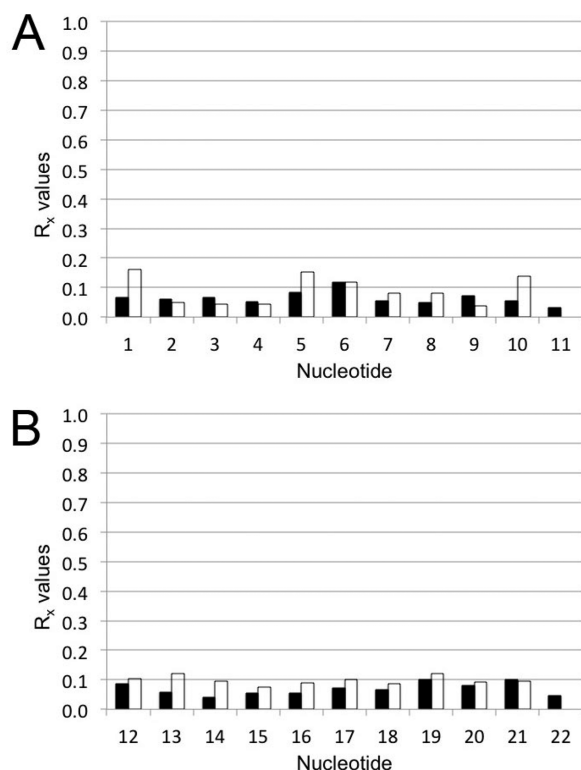


Figure 7. Complete relaxation matrix analysis (CORMA) results for internucleotide (shown in black) and intranucleotide (shown in white) NOEs for the (2*S*)-*N*⁶-HB-dA modified duplex, A (strands 1–11 and B (strands 12–22). R_1^x is the sixth root R factor: $\Sigma[(I_o)_i^{1/6} - ((I_c)_i^{1/6})/\Sigma((I_o)_i^{1/6})]$, where I_c are NOE intensities calculated from the refined structure, I_o are experimental NOE intensities.

Structure of the (2*S*)-*N*⁶-HB-dA Modified Duplex.

Figure 8 shows the average structure of the (2*S*)-*N*⁶-HB-dA modified duplex in the region of the C⁵:G¹⁸, Y⁶:T¹⁷, and A⁷:T¹⁶ base pairs. The view is from the major groove. The (2*S*)-*N*⁶-HB-dA adduct was positioned in the major groove such that the butadiene moiety oriented in the 3' direction. The C_α carbon

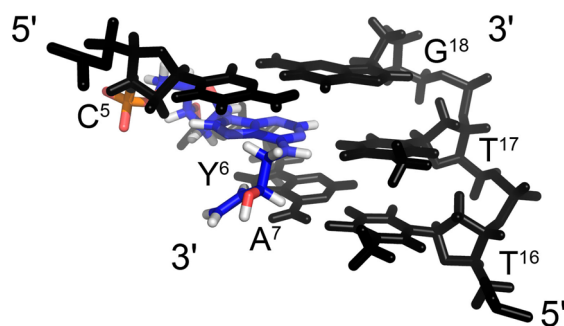


Figure 8. Average structure of the (2*S*)-*N*⁶-HB-dA modified duplex in the region of the C⁵:G¹⁸, Y⁶:T¹⁷, and A⁷:T¹⁶ base pairs. The modified nucleotide Y⁶ is shown in blue.

remained in plane with the modified nucleobase Y⁶, with the H_α and H_{α'} methylene protons facing the 5' direction, which placed the C_β carbon in the 3' direction. The C_β hydroxyl group faced the solvent, as did carbons C_γ and C_δ. There was no indication of hydrogen bond formation between the hydroxyl group at C_β with either T¹⁶ O⁴ or T¹⁷ O⁴. The (2*S*)-*N*⁶-HB-dA nucleoside maintained the *anti* conformation about the glycosyl bond. Figure 9 shows the base pairing

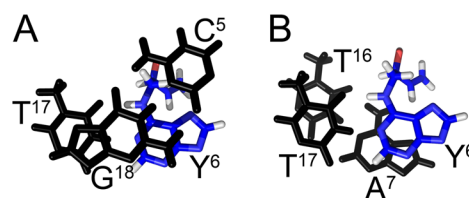


Figure 9. Stacking interactions for the (2*S*)-*N*⁶-HB-dA modified duplex. (A) Stacking of the C⁵:G¹⁸ base pair (black) above Y⁶ (blue) and T¹⁷ (black). (B) Stacking of the Y⁶:T¹⁷ pair (in blue and black, respectively) above base pair A⁷:T¹⁶ (black).

interactions at the lesion site. The modified base Y⁶ maintained Watson–Crick base pairing with the complementary base T¹⁷. The (2*S*)-*N*⁶-HB-dA adduct perturbed stacking interactions at base pairs C⁵:G¹⁸, Y⁶:T¹⁷, and A⁷:T¹⁶ (Figure 9). Thus, the Y⁶ base did not stack with its 5' neighbor C⁵, but it did with its 3' neighbor A⁷. The complementary thymine T¹⁷ stacked well with both 5' and 3' neighbors T¹⁶ and G¹⁸.

DISCUSSION

*N*⁶-HB-dA adducts induced by epoxybutene (EB, Chart 1) are of significant interest due to the ability of the BD lead to induce large numbers of mutations at A:T base pairs in DNA,^{30–34} even though alkylation of guanines by EB is more prevalent.³⁵ The origins of these adenine-specific mutations are not well understood,^{32,37,38} but their presence implies that one or more adenine-specific lesions contribute to BD-induced genotoxicity.^{32,34,36} The *N*⁶-HB-dA adducts can be formed via direct alkylation by EB of the *N*⁶-dA position or they can arise via Dimroth rearrangement of the corresponding N1-dA adducts.^{44,45} The *N*⁶-HB-dA adducts potentially interfere with Watson–Crick base pairing due to the presence of the hydroxybutenyl moiety at the *N*⁶ nitrogen, which is normally involved in hydrogen bonding with the complementary adenine. In the present study, we have prepared a DNA duplex containing the site- and stereospecific (2*S*)-*N*⁶-HB-dA adduct

opposite dT, and we have examined its effect on DNA structure and stability.

Major Groove Orientation of the (2S)-N⁶-HB-dA Adduct. The (2S)-N⁶-HB-dA adduct is positioned in the major groove of DNA. The *anti* conformation about the glycosyl bond of N⁶-HB-dA is confirmed by NOE data showing that the intensity of the NOE between Y⁶ H8 and Y⁶ H1' is small as compared to the NOE between the cytosine H5 and H6 protons (Figure 1). The (2S)-N⁶-HB-adenine base (Y⁶) maintains Watson–Crick base pairing with the complementary T¹⁷ base (Figures 8 and 10), which is confirmed by the NOE

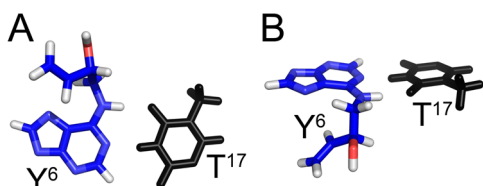
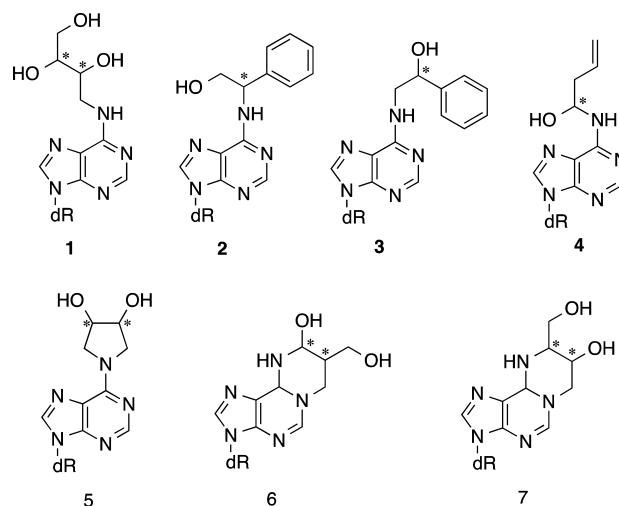


Figure 10. Y⁶:T¹⁷ base pair in the (2S)-N⁶-HB-dA duplex. (A) View from the top. (B) View from the major groove. Y⁶ forms a Watson–Crick base pair with the complementary T¹⁷ base.

cross-peak between Y⁶ H2 and T¹⁷ N3H (cross-peak g, Figure 2B). Furthermore, there is no break in the pattern of sequential NOEs between the base paired imino protons (Figure 2C), indicating that the Y⁶ base remains stacked into the DNA helix. The T¹⁶ and T¹⁷ N3H and G¹⁸ N1H imino proton resonances remain sharp as compared to the other imino proton resonances as temperature is increased (Figure 5), suggesting that the (2S)-N⁶-HB-dA lesion does not increase the rates of exchange with solvent for the C⁵:G¹⁸, Y⁶:T¹⁷, and A⁷:T¹⁶ base pair imino protons. The lower intensities of the NOE cross-peaks for base pairs G²:C²¹ and A¹⁰:T¹³ as compared to other base pair imino proton cross-peaks (Figure 2B) are attributed to their increased rate of exchange with water. Furthermore, the (2S)-N⁶-HB-dA adduct perturbs the stacking of base pair A⁷:T¹⁶ with the neighboring base pairs C⁵:G¹⁸ and Y⁶:T¹⁷ (Figure 9). The Y⁶ base does not stack well with its 5' neighbor C⁵ but does stack with its 3' neighbor A⁷, which is in the agreement with chemical shift changes for the Y⁶ H8 and H2 protons. Y⁶ H8 is shifted downfield by 0.1 ppm and Y⁶ H2 is shifted upfield by 0.15 ppm (Figure 1). The complementary thymine, T¹⁷ stacks well with both 5' and 3' neighbors T¹⁶ and G¹⁸. The 1.1 ppm chemical shift difference between the H_α and H_β resonances (Figure 3) is attributed to a stacking interaction with the C⁵ base, in which H_α is less shielded compared to that of H_β (Figure 9). Collectively, these structural perturbations may account for the 5 °C reduction in the T_m of the duplex in 0.1 M NaCl at pH 7.

Structural Comparisons to Other N⁶-dA Adducts. The structure of the (2S)-N⁶-HB-dA adduct shows significant similarities to those of N⁶-(2,3,4-trihydroxybutyl)-2'-dA (N⁶-THB-dA) adducts **1** (Chart 2) arising from another epoxide metabolite of BD, 1,2-dihydroxy-3,4-epoxybutane (EBD) (Scheme 1).^{55,56,88} Like (2S)-N⁶-HB-dA, the (2R,3R)-**1** and (2S,3S)-**1** N⁶-THB-dA adducts^{37,89} are accommodated in the major groove and maintain Watson–Crick base pairing.^{90,91} This is consistent with the facile bypass of the (2R,3R)-**1** and (2S,3S)-**1** N⁶-THB-dA adducts by *E. coli* DNA polymerases and their low mutagenicities.³⁷ Structurally, the (2S)-N⁶-HB-dA adduct differs from the N⁶-THB-dA adducts **1** due to the presence of the carbon–carbon double bond and the

Chart 2. Structures of Additional Adducts Arising from Alkylation at N⁶-dA by EBD, Styrene Oxide, and DEB



corresponding loss of the two additional hydroxyl groups of the N⁶-THB-dA adduct. For N⁶-THB-dA adducts **1**, stereospecific differences in hydrogen bonding patterns are observed for the *R,R* and the *S,S* adducts,^{37,89} which may explain the ability of the *R,R* adduct to cause A → T transversions, while the *S,S* adduct induces A → G transitions.³⁷

Our structural results for the (2S)-N⁶-HB-dA adduct are consistent with published data for N⁶-dA adducts of styrene oxide, which are also accommodated in the major groove and maintain Watson–Crick base pairing.⁹² Styrene-induced DNA alkylation can involve either the α or β carbons of styrene oxide. Feng et al.^{93,94} showed that stereochemistry at the α carbon modulates the structure of α-N⁶-dA adducts **2** of styrene oxide. For the *R* stereoisomer, the styrene ring orients in the 5'-direction in the major groove, whereas for the *S* stereoisomer, the styrene ring orients in the 3'-direction. In contrast, Hennard et al.⁹⁵ showed that the *R*- and *S*-β-N⁶-adenyl-styrene adducts **3** (Chart 2) exhibit similar major groove orientations of the styrene ring, which was attributed to the longer tether of the β adducts. Site-specific mutagenesis studies of these regioisomeric N⁶-dA styrene oxide adducts also indicate low levels of mutations.⁹⁶

The observed structural similarities between the (2S)-N⁶-HB-dA adduct investigated here and other known N⁶-dA adducts predict that the (2S)-N⁶-HB-dA adduct will be weakly mutagenic. Detailed site-specific mutagenesis studies have not been reported for (2S)-N⁶-HB-dA. However, Carmical et al.³⁷ reported that regioisomeric (1R)-N⁶-HB-dA and (1S)-N⁶-HB-dA adducts **4** (Chart 2) were nonmutagenic in *Escherichia coli*.³⁷

The minor effects of (2S)-N⁶-HB-dA adducts on DNA structure are in contrast with the more pronounced distortions induced by the bis-alkylation products at N⁶-dA induced by diepoxybutane (DEB): N⁶,N⁶-(2,3-dihydroxybutan-1,4-diyl)-2'-deoxyadenosine (N⁶,N⁶-DHB-dA in Chart 2). Two enantiomers of N⁶,N⁶-DHB-dA have been identified in DNA: *R,R*-**5** and *S,S*-**5**.^{97,98} NMR structures of *R,R*- and *S,S*-**5** in the ras61 sequence^{97,98} revealed that the 3,4-dihydroxypyrrolidine ring is localized in the major groove but rotates around the C6-N⁶ bond, allowing for the complementary thymine to remain inserted in the DNA duplex. In contrast to the (2S)-N⁶-HB-dA adduct, *R,R*- and *S,S*-**5** form only one Watson–Crick hydrogen

bond to the complementary thymine between the adenine N1 imino nitrogen and the T¹⁷ N3H imino proton of the complementary strand.⁹⁸ As compared to the (2S)-N⁶-HB-dA adduct, the R,R- and S,S-5 adducts significantly destabilize the duplex, evidenced by a 16–17 °C decrease in T_m.⁹⁹ Replication studies conducted *in vitro* have revealed that the DHB-dA adducts block human DNA polymerase β and are bypassed in an error-prone manner by human translesion synthesis (TLS) polymerases κ and η, leading to both base substitution and deletion mutations.¹⁰⁰ Studies are in progress to evaluate polymerase bypass and mutagenicity of the (2S)-N⁶-HB-dA adduct.

SUMMARY

Detailed solution NMR studies reveal that the (2S)-N⁶-HB-dA adduct is positioned in the major groove of DNA. This adduct maintains Watson–Crick base pairing with the complementary T¹⁷ base and is stacked into the helix. The (2S)-N⁶-HB-dA base does not increase the rates of exchange with solvent for the C⁵:G¹⁸, Y⁶:T¹⁷, and A⁷:T¹⁶ base pairs. It modestly perturbs base stacking interactions at base pairs C⁵:G¹⁸, Y⁶:T¹⁷, and A⁷:T¹⁶, which when combined with the accommodation of the adduct in the major groove, may account for the 5 °C reduction in the T_m of the duplex in 0.1 M NaCl at pH 7.

ASSOCIATED CONTENT

Supporting Information

Parameters for the (2S)-N⁶-HB-dA adduct used in rMD calculations; chemical shifts of the nonexchangeable protons of the (2S)-N⁶-HB-dA modified duplex; and chemical shifts of the nonexchangeable protons in the (2S)-N⁶-HB-dA modified duplex. This material is available free of charge via the Internet at <http://pubs.acs.org>.

AUTHOR INFORMATION

Corresponding Author

*Tel: 615-322-2589. E-mail: michael.p.stone@vanderbilt.edu.

Funding

This work was supported by NIH grants R01 ES-05509 (to M.P.S.) and CA-100670 (to N.T.). The Vanderbilt University Center in Molecular Toxicology was supported by NIH grant P30 ES-00267. The Vanderbilt Ingram Cancer Center was funded by NIH grant P30 CA-68485. Funding for NMR was supplied by NIH grants S10 RR-05805, S10 RR-025677, and NSF Grant DBI 0922862, the latter funded by the American Recovery and Reinvestment Act of 2009 (Public Law 111-5). Vanderbilt University assisted with the purchase of NMR instrumentation.

Notes

The authors declare no competing financial interest.

ABBREVIATIONS

dA, 2'-deoxyadenosine; BD, 1,3-butadiene; BDT, butadiene triol; CORMA, correlated matrix analysis; COSY, correlated spectroscopy; DIPEA, N,N-diisopropylethyl amine; DMSO, dimethyl sulfoxide; dR, 2'-deoxyribose; DSS, 4,4-dimethyl-4-silapentane-1-sulfonic acid; DEB, 1,2,3,4-diepoxybutane; EB, 1,2-epoxy-3-butene; EBD, 1,2-dihydroxy-3,4-epoxybutane; HPLC, high pressure liquid chromatography; HPLC–ESI–MS, high pressure liquid chromatography–electrospray ionization–mass spectrometry; MALDI–TOF–MS, matrix-assisted laser desorption/ionization time-of-flight mass spectrometry;

N⁶-HB-dA, N⁶-(2-hydroxy-3-buten-1-yl)-2'-deoxyadenosine; R₁^x, sixth root residual; rMD, restrained molecular dynamics; rmsd, root-mean-square deviation; NOESY, nuclear Overhauser effect spectroscopy

REFERENCES

- (1) Huff, J. E., Melnick, R. L., Solleveld, H. A., Haseman, J. K., Powers, M., and Miller, R. A. (1985) Multiple organ carcinogenicity of 1,3-butadiene in B6c3F1 mice after 60 weeks of inhalation exposure. *Science* 227, 548–549.
- (2) Melnick, R. L., Huff, J., Chou, B. J., and Miller, R. A. (1990) Carcinogenicity of 1,3-butadiene in C57BL/6 x C3H F1 mice at low exposure concentrations. *Cancer Res.* 50, 6592–6599.
- (3) Melnick, R. L., Huff, J. E., Roycroft, J. H., Chou, B. J., and Miller, R. A. (1990) Inhalation toxicology and carcinogenicity of 1,3-butadiene in B6c3F1 mice following 65 weeks of exposure. *Environ. Health Perspect.* 86, 27–36.
- (4) Owen, P. E., and Glaister, J. R. (1990) Inhalation toxicity and carcinogenicity of 1,3-butadiene in Sprague-Dawley rats. *Environ. Health Perspect.* 86, 19–25.
- (5) United States Environmental Protection Agency (EPA). (2002) *Health Assessment of 1,3-Butadiene*, EPA/600/P-98/001F, National Center for Environmental Assessment, Washington, DC, available from National Technical Information Service, Springfield, VA, <http://www.epa.gov/ncea/>.
- (6) National Toxicology Program (NTP). (2011) 1,3-Butadiene, CAS No. 106-99-0, in *12th Report on Carcinogens (RoC)*, National Toxicology Program, Research Triangle Park, NC, <http://ntp.niehs.nih.gov/go/roc12>.
- (7) IARC (1999) Re-evaluation of some organic chemicals, hydrazine and hydrogen peroxide. *IARC Sci. Publ.* 71, 109–125.
- (8) International Agency for Research on Cancer (2008) 1,3-Butadiene, ethylene oxide and vinyl halides (vinyl fluoride, vinyl chloride and vinyl bromide). *IARC Monogr. Eval. Carcinog. Risks Hum.* 97, 3–471.
- (9) Swenberg, J. A., Bordeerat, N. K., Boysen, G., Carro, S., Georgieva, N. I., Nakamura, J., Troutman, J. M., Upton, P. B., Albertini, R. J., Vacek, P. M., Walker, V. E., Sram, R. J., Goggin, M., and Tretyakova, N. (2011) 1,3-Butadiene: Biomarkers and application to risk assessment. *Chem.-Biol. Interact.* 192, 150–154.
- (10) Kotapati, S., Sangaraju, D., Esades, A., Hallberg, L., Walker, V. E., Swenberg, J. A., and Tretyakova, N. Y. (2014) Bis-butenediol-mercaptopuric acid (bis-BDMA) as a urinary biomarker of metabolic activation of butadiene to its ultimate carcinogenic species. *Carcinogenesis* 35, 1371–1378.
- (11) Himmelstein, M. W., Acquavella, J. F., Recio, L., Medinsky, M. A., and Bond, J. A. (1997) Toxicology and epidemiology of 1,3-butadiene. *Crit. Rev. Toxicol.* 27, 1–108.
- (12) Jackson, M. A., Stack, H. F., Rice, J. M., and Waters, M. D. (2000) A review of the genetic and related effects of 1,3-butadiene in rodents and humans. *Mutat. Res.* 463, 181–213.
- (13) Pelz, N., Dempster, N. M., and Shore, P. R. (1990) Analysis of low molecular weight hydrocarbons including 1,3-butadiene in engine exhaust gases using an aluminum oxide porous-layer open-tubular fused-silica column. *J. Chromatogr. Sci.* 28, 230–235.
- (14) Brunnemann, K. D., Kagan, M. R., Cox, J. E., and Hoffmann, D. (1990) Analysis of 1,3-butadiene and other selected gas-phase components in cigarette mainstream and sidestream smoke by gas chromatography-mass selective detection. *Carcinogenesis* 11, 1863–1868.
- (15) Ward, J. B., Jr., Ammenheuser, M. M., Bechtold, W. E., Whorton, E. B., Jr., and Legator, M. S. (1994) hprt mutant lymphocyte frequencies in workers at a 1,3-butadiene production plant. *Environ. Health Perspect.* 102 (Suppl 9), 79–85.
- (16) Ward, J. B., Jr., Ammenheuser, M. M., Whorton, E. B., Jr., Bechtold, W. E., Kelsey, K. T., and Legator, M. S. (1996) Biological monitoring for mutagenic effects of occupational exposure to butadiene. *Toxicology* 113, 84–90.

- (17) Sram, R. J., Rossner, P., Peltonen, K., Podrazilova, K., Mrackova, G., Demopoulos, N. A., Stephanou, G., Vlachodimitropoulos, D., Darroudi, F., and Bates, A. D. (1998) Chromosomal aberrations, sister-chromatid exchanges, cells with high frequency of SCE, micronuclei and comet assay parameters in 1,3-butadiene-exposed workers. *Mutat. Res.* 419, 145–154.
- (18) Meinhardt, T. J., Lemen, R. A., Crandall, M. S., and Young, R. J. (1982) Environmental epidemiologic investigation of the styrene-butadiene rubber industry. Mortality patterns with discussion of the hematopoietic and lymphatic malignancies. *Scand. J. Work Environ. Health* 8, 250–259.
- (19) Matanoski, G. M., and Schwartz, L. (1987) Mortality of workers in styrene-butadiene polymer production. *J. Occup. Med.* 29, 675–680.
- (20) Santos-Burgoa, C., Matanoski, G. M., Zeger, S., and Schwartz, L. (1992) Lymphohematopoietic cancer in styrene-butadiene polymerization workers. *Am. J. Epidemiol.* 136, 843–854 (see comments).
- (21) Matanoski, G., Francis, M., Correa-Villasenor, A., Elliott, E., Santos-Burgoa, C., and Schwartz, L. (1993) Cancer epidemiology among styrene-butadiene rubber workers. *IARC Sci. Publ.* 127, 363–374.
- (22) Delzell, E., Sathiakumar, N., Hovinga, M., Macaluso, M., Julian, J., Larson, R., Cole, P., and Muir, D. C. (1996) A follow-up study of synthetic rubber workers. *Toxicology* 113, 182–189.
- (23) Macaluso, M., Larson, R., Delzell, E., Sathiakumar, N., Hovinga, M., Julian, J., Muir, D., and Cole, P. (1996) Leukemia and cumulative exposure to butadiene, styrene and benzene among workers in the synthetic rubber industry. *Toxicology* 113, 190–202.
- (24) Santos-Burgoa, C., Eden-Wynter, R. A., Riojas-Rodriguez, H., and Matanoski, G. M. (1997) Living in a chemical world. Health impact of 1,3-butadiene carcinogenesis. *Ann. N.Y. Acad. Sci.* 837, 176–188.
- (25) Matanoski, G., Elliott, E., Tao, X., Francis, M., Correa-Villasenor, A., and Santos-Burgoa, C. (1997) Lymphohematopoietic cancers and butadiene and styrene exposure in synthetic rubber manufacture. *Ann. N.Y. Acad. Sci.* 837, 157–169.
- (26) Albertini, R., Clewell, H., Himmelstein, M. W., Morinello, E., Olin, S., Preston, J., Scarano, L., Smith, M. T., Swenberg, J., Tice, R., and Travis, C. (2003) The use of non-tumor data in cancer risk assessment: Reflections on butadiene, vinyl chloride, and benzene. *Regul. Toxicol. Pharmacol.* 37, 105–132.
- (27) Kirman, C. R., Albertini, R. J., Sweeney, L. M., and Gargas, M. L. (2010) 1,3-Butadiene: I. Review of metabolism and the implications to human health risk assessment. *Crit. Rev. Toxicol.* 40 (Suppl 1), 1–11.
- (28) Albertini, R. J., Carson, M. L., Kirman, C. R., and Gargas, M. L. (2010) 1,3-Butadiene: II. Genotoxicity profile. *Crit. Rev. Toxicol.* 40 (Suppl 1), 12–73.
- (29) Kirman, C. R., Albertini, R. A., and Gargas, M. L. (2010) 1,3-Butadiene: III. Assessing carcinogenic modes of action. *Crit. Rev. Toxicol.* 40 (Suppl 1), 74–92.
- (30) Cochrane, J. E., and Skopek, T. R. (1993) Mutagenicity of 1,3-Butadiene and Its Epoxide Metabolites in Human TK6 Cells and in Splenic T Cells Isolated from Exposed C6c3F1 Mice, in *Butadiene and Styrene, Assessment of Health Hazards*, Vol. 127, pp 195–204, IARC, Lyon, France.
- (31) Cochrane, J. E., and Skopek, T. R. (1994) Mutagenicity of butadiene and its epoxide metabolites: I. Mutagenic potential of 1,2-epoxybutene, 1,2,3,4-diepoxybutane and 3,4-epoxy-1,2-butanediol in cultured human lymphoblasts. *Carcinogenesis* 15, 713–717.
- (32) Cochrane, J. E., and Skopek, T. R. (1994) Mutagenicity of butadiene and its epoxide metabolites: II. Mutational spectra of butadiene, 1,2-epoxybutene and diepoxybutane at the hprt locus in splenic T cells from exposed B6c3F1 mice. *Carcinogenesis* 15, 719–723.
- (33) Recio, L., Saranko, C. J., and Steen, A. M. (2000) 1,3-butadiene: Cancer, mutations, and adducts. Part II: Roles of two metabolites of 1,3-butadiene in mediating its *in vivo* genotoxicity. *Res. Rep. - Health Eff. Inst.*, 49–87 discussion 141–149.
- (34) Recio, L., Steen, A. M., Pluta, L. J., Meyer, K. G., and Saranko, C. J. (2001) Mutational spectrum of 1,3-butadiene and metabolites 1,2-epoxybutene and 1,2,3,4-diepoxybutane to assess mutagenic mechanisms. *Chem.-Biol. Interact.* 135–136, 325–341.
- (35) Lawley, P. D., and Brookes, P. (1967) Interstrand cross-linking of DNA by difunctional alkylating agents. *J. Mol. Biol.* 25, 143–160.
- (36) Steen, A. M., Meyer, K. G., and Recio, L. (1997) Analysis of hprt mutations occurring in human TK6 lymphoblastoid cells following exposure to 1,2,3,4-diepoxybutane. *Mutagenesis* 12, 61–67.
- (37) Carmical, J. R., Nechev, L. V., Harris, C. M., Harris, T. M., and Lloyd, R. S. (2000) Mutagenic potential of adenine N⁶ adducts of monoepoxide and diepoxy derivatives of butadiene. *Environ. Mol. Mutagen.* 35, 48–56.
- (38) Scholdberg, T. A., Nechev, L. V., Merritt, W. K., Harris, T. M., Harris, C. M., Lloyd, R. S., and Stone, M. P. (2005) Mispairing of a site specific major groove (2S,3S)-N⁶-(2,3,4-trihydroxybutyl)-2'-deoxyadenosyl DNA adduct of butadiene diol epoxide with deoxyguanosine: Formation of a dA(anti):dG(anti) pairing interaction. *Chem. Res. Toxicol.* 18, 145–153.
- (39) Tretyakova, N., Lin, Y., Sangaiah, R., Upton, P. B., and Swenberg, J. A. (1997) Identification and quantitation of DNA adducts from calf thymus DNA exposed to 3,4-epoxy-1-butene. *Carcinogenesis* 18, 137–147.
- (40) Csanady, G. A., Guengerich, F. P., and Bond, J. A. (1992) Comparison of the biotransformation of 1,3-butadiene and its metabolite, butadiene monoepoxide, by hepatic and pulmonary tissues from humans, rats and mice. *Carcinogenesis* 13, 1143–1153 (published erratum appears in (1993) *Carcinogenesis* 14 (4) 784).
- (41) Duescher, R. J., and Elfarra, A. A. (1994) Human liver microsomes are efficient catalysts of 1,3-butadiene oxidation: Evidence for major roles by cytochromes P450 2A6 and 2E1. *Arch. Biochem. Biophys.* 311, 342–349.
- (42) Koivisto, P., Kostianen, R., Kilpelainen, I., Steinby, K., and Peltonen, K. (1995) Preparation, characterization and ³²P-postlabeling of butadiene monoepoxide N⁶-adenine adducts. *Carcinogenesis* 16, 2999–3007.
- (43) Engel, J. D. (1975) Mechanism of the Dimroth rearrangement in adenosine. *Biochem. Biophys. Res. Commun.* 64, 581–586.
- (44) Qian, C., and Dipple, A. (1995) Different mechanisms of aralkylation of adenosine at the 1- and N⁶- positions. *Chem. Res. Toxicol.* 8, 389–395.
- (45) Kim, H. Y., Finneman, J. L., Harris, C. M., and Harris, T. M. (2000) Studies of the mechanisms of adduction of 2'-deoxyadenosine with styrene oxide and polycyclic aromatic hydrocarbon dihydrodiol epoxides. *Chem. Res. Toxicol.* 13, 625–637.
- (46) Koivisto, P., Adler, I. D., Sorsa, M., and Peltonen, K. (1996) Inhalation exposure of rats and mice to 1,3-butadiene induces N⁶-adenine adducts of epoxybutene detected by ³²P-postlabeling and HPLC. *Environ. Health Perspect.* 104, 655–657.
- (47) Selzer, R. R., and Elfarra, A. A. (1999) *In vitro* reactions of butadiene monoxide with single- and double-stranded DNA: Characterization and quantitation of several purine and pyrimidine adducts. *Carcinogenesis* 20, 285–292.
- (48) Koivisto, P., Adler, I. D., Pacchierotti, F., and Peltonen, K. (1998) DNA adducts in mouse testis and lung after inhalation exposure to 1,3-butadiene. *Mutat. Res.* 397, 3–10.
- (49) Ristau, C., Deutschmann, S., Laib, R. J., and Ottenwalder, H. (1990) Detection of diepoxybutane-induced DNA-DNA crosslinks by cesium trifluoroacetate (CsTFA) density-gradient centrifugation. *Arch. Toxicol.* 64, 343–344.
- (50) Vangala, R. R., Laib, R. J., and Bolt, H. M. (1993) Evaluation of DNA damage by alkaline elution technique after inhalation exposure of rats and mice to 1,3-butadiene. *Arch. Toxicol.* 67, 34–38.
- (51) Goggin, M., Loeber, R., Park, S., Walker, V., Wickliffe, J., and Tretyakova, N. (2007) HPLC-ESI+-MS/MS analysis of N7-guanine-N7-guanine DNA cross-links in tissues of mice exposed to 1,3-butadiene. *Chem. Res. Toxicol.* 20, 839–847.
- (52) Goggin, M., Anderson, C., Park, S., Swenberg, J., Walker, V., and Tretyakova, N. (2008) Quantitative high-performance liquid chromatography-electrospray ionization-tandem mass spectrometry analysis of

the adenine-guanine cross-links of 1,2,3,4-diepoxybutane in tissues of butadiene-exposed B6C3F1 mice. *Chem. Res. Toxicol.* 21, 1163–1170.

(53) Goggin, M., Swenberg, J. A., Walker, V. E., and Tretyakova, N. (2009) Molecular dosimetry of 1,2,3,4-diepoxybutane-induced DNA-DNA cross-links in B6C3F1 mice and F344 rats exposed to 1,3-butadiene by inhalation. *Cancer Res.* 69, 2479–2486.

(54) Sangaraju, D., Goggin, M., Walker, V., Swenberg, J., and Tretyakova, N. (2012) NanoHPLC-nanoESI(+)-MS/MS quantitation of bis-N7-guanine DNA-DNA cross-links in tissues of B6C3F1 mice exposed to subppm levels of 1,3-butadiene. *Anal. Chem.* 84, 1732–1739.

(55) Malvoisin, E., and Roberfroid, M. (1982) Hepatic microsomal metabolism of 1,3-butadiene. *Xenobiotica* 12, 137–144.

(56) Cheng, X., and Ruth, J. A. (1993) A simplified methodology for quantitation of butadiene metabolites. Application to the study of 1,3-butadiene metabolism by rat liver microsomes. *Drug Metab. Dispos.* 21, 121–124.

(57) Nauhaus, S. K., Fennell, T. R., Asgharian, B., Bond, J. A., and Sumner, S. C. (1996) Characterization of urinary metabolites from Sprague-Dawley rats and B6C3F1 mice exposed to [1,2,3,4-¹³C]-butadiene. *Chem. Res. Toxicol.* 9, 764–773.

(58) Kemper, R. A., Elfarrar, A. A., and Myers, S. R. (1998) Metabolism of 3-butene-1,2-diol in B6C3F1 mice. Evidence for involvement of alcohol dehydrogenase and cytochrome P450. *Drug Metab. Dispos.* 26, 914–920.

(59) Powley, M. W., Jayaraj, K., Gold, A., Ball, L. M., and Swenberg, J. A. (2003) 1,N²-Propanodeoxyguanosine adducts of the 1,3-butadiene metabolite, hydroxymethylvinyl ketone. *Chem. Res. Toxicol.* 16, 1448–1454.

(60) Geacintov, N. E., Cosman, M., Hingerty, B. E., Amin, S., Broyde, S., and Patel, D. J. (1997) NMR solution structures of stereoisomeric covalent polycyclic aromatic carcinogen-DNA adducts: Principles, patterns and diversity. *Chem. Res. Toxicol.* 10, 111–146.

(61) Nechev, L. V., Zhang, M., Tsarouhtsis, D., Tamura, P. J., Wilkinson, A. S., Harris, C. M., and Harris, T. M. (2001) Synthesis and characterization of nucleosides and oligonucleotides bearing adducts of butadiene epoxides on adenine N⁶ and guanine N². *Chem. Res. Toxicol.* 14, 379–388.

(62) Kim, S. J., Stone, M. P., Harris, C. M., and Harris, T. M. (1992) A postoligomerization synthesis of oligodeoxynucleotides containing polycyclic aromatic hydrocarbon adducts at the N⁶ position of deoxyadenosine. *J. Am. Chem. Soc.* 114, 5480–5481.

(63) Kim, H.-Y., Nechev, L., Zhou, L., Tamura, P., Harris, C. M., and Harris, T. M. (1998) Synthesis and adduction of fully deprotected oligodeoxynucleotides containing 6-chloropurine. *Tetrahedron Lett.* 39, 6803–6806.

(64) Dorr, D. Q., Murphy, K., and Tretyakova, N. (2006) Synthesis of DNA oligodeoxynucleotides containing structurally defined N⁶-(2-hydroxy-3-buten-1-yl)-adenine adducts of 3,4-epoxy-1-butene. *Chem.-Biol. Interact.* 166, 104–111.

(65) Feng, B., and Stone, M. P. (1995) Solution structure of an oligodeoxynucleotide containing the human N-ras codon 61 sequence refined from ¹H NMR using molecular dynamics restrained by nuclear Overhauser effects. *Chem. Res. Toxicol.* 8, 821–832.

(66) Cavaluzzi, M. J., and Borer, P. N. (2004) Revised UV extinction coefficients for nucleoside-5'-monophosphates and unpaired DNA and RNA. *Nucleic Acids Res.* 32, e13.

(67) Jeener, J., Meier, B. H., Bachmann, P., and Ernst, R. R. (1979) Investigation of exchange processes by 2-dimensional NMR spectroscopy. *J. Chem. Phys.* 71, 4546–4553.

(68) Wagner, R., and Berger, S. (1996) Gradient-selected NOESY - A fourfold reduction of the measurement time for the NOESY experiment. *J. Magn. Reson., Ser. A* 123, 119–121.

(69) Piantini, U., Sorensen, O. W., and Ernst, R. R. (1982) Multiple quantum filters for elucidating NMR coupling networks. *J. Am. Chem. Soc.* 104, 6800–6801.

(70) Piatto, M., Saudek, V., and Sklenar, V. (1992) Gradient-tailored excitation for single-quantum NMR spectroscopy of aqueous solutions. *J. Biomol. NMR* 6, 661–665.

(71) Goddard, T. D., and Kneller, D. G. (2006) SPARKY v. 3.113, University of California, San Francisco, San Francisco, CA.

(72) Frisch, M. J., Trucks, G. W., Schlegel, H. B., Scuseria, G. E., Robb, M. A., Cheeseman, J. R., Scalmani, G., Barone, V., Mennucci, B., Petersson, G. A., Nakatsuji, H., Caricato, M., Li, X., Hratchian, H. P., Izmaylov, A. F., Bloino, J., Zheng, G., Sonnenberg, J. L., Hada, M., Ehara, M., Toyota, K., Fukuda, R., Hasegawa, J., Ishida, M., Nakajima, T., Honda, Y., Kitao, O., Nakai, H., Vreven, T., Montgomery, J. A., Peralta, J. E., Ogliaro, F., Bearpark, M., Heyd, J. J., Brothers, E., Kudin, K. N., Staroverov, V. N., Kobayashi, R., Normand, J., Raghavachari, K., Rendell, A., Burant, J. C., Iyengar, S. S., Tomasi, J., Cossi, M., Rega, N., Millam, J. M., Klene, M., Knox, J. E., Cross, J. B., Bakken, V., Adarno, C., Jaramillo, J., Gomperts, R., Stratmann, R. E., Yazyev, O., Austin, A. J., Cammi, R., Pomelli, C., Ochterski, J. W., Martin, R. L., Morokuma, K., Zakrzewski, V. G., Voth, G. A., Salvador, P., Dannenberg, J. J., Dapprich, S., Daniels, A. D., Foresman, J. B., Ortiz, J. V., Cioslowski, J., and Fox, D. J. (2009) *Gaussian 09*, Gaussian, Inc., Wallingford, CT.

(73) Schafmeister, C. E. A., Ross, W. S., and Romanovski, V. (1995) XLEAP, University of California, San Francisco, San Francisco, CA.

(74) Keepers, J. W., and James, T. L. (1984) A theoretical study of distance determination from NMR. Two-dimensional nuclear Overhauser effect spectra. *J. Magn. Reson.* 57, 404–426.

(75) James, T. L. (1991) Relaxation matrix analysis of two-dimensional nuclear Overhauser effect spectra. *Curr. Opin. Struct. Biol.* 1, 1042–1053.

(76) Borgias, B. A., and James, T. L. (1990) MARDIGRAS—a procedure for matrix analysis of relaxation for discerning geometry of an aqueous structure. *J. Magn. Reson.* 87, 475–487.

(77) Tonelli, M., and James, T. L. (1998) Insights into the dynamic nature of DNA duplex structure via analysis of nuclear Overhauser effect intensities. *Biochemistry* 37, 11478–11487.

(78) Arnott, S., and Hukins, D. W. L. (1972) Optimised parameters for A-DNA and B-DNA. *Biochem. Biophys. Res. Commun.* 47, 1504–1509.

(79) Kirkpatrick, S., Gelatt, C. D., Jr., and Vecchi, M. P. (1983) Optimization by simulated annealing. *Science* 220, 671–680.

(80) Case, D. A., Cheatham, T. E., III, Darden, T., Gohlke, H., Luo, R., Merz, K. M., Jr., Onufriev, A., Simmerling, C., Wang, B., and Woods, R. J. (2005) The AMBER biomolecular simulation programs. *J. Comput. Chem.* 26, 1668–1688.

(81) Wang, J. M., Cieplak, P., and Kollman, P. A. (2000) How well does a restrained electrostatic potential (RESP) model perform in calculating conformational energies of organic and biological molecules? *J. Comput. Chem.* 21, 1049–1074.

(82) Bashford, D., and Case, D. A. (2000) Generalized Born models of macromolecular solvation effects. *Annu. Rev. Phys. Chem.* 51, 129–152.

(83) Berendsen, H. J. C., Postma, J. P. M., van Gunsteren, W. F., DiNola, A., and Haak, J. R. (1984) Molecular dynamics with coupling to an external bath. *J. Phys. Chem.* 81, 3684–3690.

(84) Patel, D. J., Shapiro, L., and Hare, D. (1987) DNA and RNA: NMR studies of conformations and dynamics in solution. *Q. Rev. Biophys.* 20, 35–112.

(85) Reid, B. R. (1987) Sequence-specific assignments and their use in NMR studies of DNA structure. *Q. Rev. Biophys.* 20, 2–28.

(86) Boelens, R., Scheek, R. M., Dijkstra, K., and Kaptein, R. (1985) Sequential assignment of imino- and amino-proton resonances in ¹H NMR spectra of oligonucleotides by two-dimensional NMR spectroscopy. Application to a lac operator fragment. *J. Magn. Reson.* 62, 378–386.

(87) Nilges, M., Clore, G. M., and Gronenborn, A. M. (1988) Determination of three-dimensional structures of proteins from interproton distance data by dynamical simulated annealing from a random array of atoms. Circumventing problems associated with folding. *FEBS Lett.* 239, 129–136.

(88) Boogaard, P. J., and Bond, J. A. (1996) The role of hydrolysis in the detoxification of 1,2:3,4-diepoxybutane by human, rat, and mouse liver and lung *in vitro*. *Toxicol. Appl. Pharmacol.* 141, 617–627.

(89) Carmical, J. R., Kowalczyk, A., Zou, Y., Van Houten, B., Nechev, L. V., Harris, C. M., Harris, T. M., and Lloyd, R. S. (2000) Butadiene-induced intrastrand DNA cross-links: A possible role in deletion mutagenesis. *J. Biol. Chem.* 275, 19482–19489.

(90) Merritt, W. K., Scholdberg, T. A., Nechev, L. V., Harris, T. M., Harris, C. M., Lloyd, R. S., and Stone, M. P. (2004) Stereospecific structural perturbations arising from adenine N^6 butadiene triol adducts in duplex DNA. *Chem. Res. Toxicol.* 17, 1007–1019.

(91) Scholdberg, T. A., Nechev, L. V., Merritt, W. K., Harris, T. M., Harris, C. M., Lloyd, R. S., and Stone, M. P. (2004) Structure of a site specific major groove (2S,3S)- N^6 -(2,3,4-trihydroxybutyl)-2'-deoxyadenosyl DNA adduct of butadiene diol epoxide. *Chem. Res. Toxicol.* 17, 717–730.

(92) Stone, M. P., and Feng, B. (1996) Sequence and stereospecific consequences of major groove (N^6 -adenyl)-styrene oxide adducts in an oligodeoxynucleotide containing the human *N-ras* codon 61 sequence. *Magn. Reson. Chem.* 34, S105–S114.

(93) Feng, B., Zhou, L., Passarelli, M., Harris, C. M., Harris, T. M., and Stone, M. P. (1995) Major groove (R)- α -(N^6 -adenyl)styrene oxide adducts in an oligodeoxynucleotide containing the human *N-ras* codon 61 sequence: Conformations of the R(61,2) and R(61,3) sequence isomers from ^1H NMR. *Biochemistry* 34, 14021–14036.

(94) Feng, B., Voehler, M., Zhou, L., Passarelli, M., Harris, C. M., Harris, T. M., and Stone, M. P. (1996) Major groove (S)- α -(N^6 -adenyl)styrene oxide adducts in an oligodeoxynucleotide containing the human *N-ras* codon 61 sequence: Conformations of the S(61,2) and S(61,3) sequence isomers from ^1H NMR. *Biochemistry* 35, 7316–7329.

(95) Hennard, C., Finneman, J., Harris, C. M., Harris, T. M., and Stone, M. P. (2001) The nonmutagenic (R)- and (S)- β -(N^6 -adenyl)styrene oxide adducts are oriented in the major groove and show little perturbation to DNA structure. *Biochemistry* 40, 9780–9791.

(96) Latham, G. J., Zhou, L., Harris, C. M., Harris, T. M., and Lloyd, R. S. (1993) The replication fate of R- and S-styrene oxide adducts on adenine N^6 is dependent on both the chirality of the lesion and the local sequence context. *J. Biol. Chem.* 268, 23427–23434.

(97) Seneviratne, U., Antsyovich, S., Goggin, M., Dorr, D. Q., Guza, R., Moser, A., Thompson, C., York, D. M., and Tretyakova, N. (2010) Exocyclic deoxyadenosine adducts of 1,2,3,4-diepoxybutane: Synthesis, structural elucidation, and mechanistic studies. *Chem. Res. Toxicol.* 23, 118–133.

(98) Kowal, E. A., Seneviratne, U., Wickramaratne, S., Doherty, K. E., Cao, X., Tretyakova, N., and Stone, M. P. (2014) Structures of exocyclic R,R- and S,S N^6,N^6 -(2,3-dihydroxy-1,4-butadiyl)-2'-deoxyadenosine adducts induced by 1,2,3,4-diepoxybutane. *Chem. Res. Toxicol.* 27, 805–817.

(99) Seneviratne, U., Antsyovich, S., Dorr, D. Q., Dissanayake, T., Kotapati, S., and Tretyakova, N. (2010) DNA oligomers containing site-specific and stereospecific exocyclic deoxyadenosine adducts of 1,2,3,4-diepoxybutane: Synthesis, characterization, and effects on DNA structure. *Chem. Res. Toxicol.* 23, 1556–1567.

(100) Kotapati, S., Maddukuri, L., Wickramaratne, S., Seneviratne, U., Pence, M., Marnett, L., and Tretyakova, N. (2012) *Translesion Synthesis Across 1,3-Butadiene-Induced Deoxyadenosine Adducts [Abstract]*, Division of Chemical Toxicology, 244th National Meeting of the American Chemical Society, Philadelphia, PA, Aug 19–23, American Chemical Society, Washington, DC.